NASA/TM— 207382

IN-76-TM
067649

Bulk Growth of Wide Band Gap II-VI Compound Semiconductors by Physical Vapor Transport

Ching-Hua Su

Space Science Laboratory, NASA/Marshall Space Flight Center,

Huntsville, Alabama USA

ABSTRACT

The mechanism of physical vapor transport of II-VI semiconducting compounds was studied both theoretically, using a one-dimensional diffusion model, as well as experimentally. It was found that the vapor phase stoichiometry is critical in determining the vapor transport rate. The experimental heat treatment methods to control the vapor composition over the starting materials were investigated and the effectiveness of the heat treatments was confirmed by partial pressure measurements using an optical absorption technique. The effect of residual (foreign) gas on the transport rate was also studies theoretically by the diffusion model and confirmed experimentally by the measurements of total pressure and compositions of the residual gas. An in-situ dynamic technique for the transport rate measurements and a further extension of the technique that simultaneously measured the partial pressures and transport rates were performed and, for the first time, the experimentally determined mass fluxes were compared with those calculated, without any adjustable parameters, from the diffusion model. Using the information obtained from the experimental transport rate measurements as guideline high quality bulk crystal of wide band gap II-VI semiconductor were grown from the source materials which undergone the same heat treatment methods. The grown crystals were then extensively characterized with emphasis on the analysis of the crystalline structural defects.

Keywords: Physical Vapor Transport (PVT), II-VI Compound Semiconductors

1. INTRODUCTION

The studies on the crystal growth and characterization of II-VI wide band gap compound semiconductors, such as ZnTe, CdS, ZnSe and ZnS, have been conducted over the past three decades. The research was not quite as extensive as that on Si, III-V, or even narrow band gap II-VI semiconductors because of the high melting temperatures as well as the specialized applications associated with these wide band gap semiconductors. In the past several years, major advances in the thin film technology such as molecular beam epitaxy (MBE) and metal organic chemical vapor deposition (MOCVD) have demonstrated the applications of these materials for the important devices such as light-emitting diode [1], laser [2] and ultraviolet detectors [3] and the tunability of energy band gap by employing ternary [4] or even quaternary systems [5] of these compounds. At the same time, the development in the crystal growth of bulk materials has not advanced far enough to provide low price, high quality substrates needed for the thin film growth technology [6].

Crystallization from vapor has various advantages over melt growth. These advantages result mostly from (1) the lower processing temperature involved — the high melting temperatures of these materials make the melt growth process very difficult to handle, (2) physical vapor transport acts as a purification process [7] because of the differences in the vapor pressures of the native elements and the impurities, and (3) most solid-vapor interfaces exhibit higher interfacial morphological stability [8] during growth because of their low atomic roughness [9] and, consequently, the pronounced growth rate anisotropy. The technique of physical vapor transport in closed ampoules is especially attractive for space investigation due to its experimental simplicity and minimal needs for complex process control. In this paper, we will discuss the activities of bulk growth of these wide band gap II-VI semiconductors by physical vapor transport (PVT) technique developed in our laboratory during the past years.

The main disadvantage of vapor growth technique compared to other growth technique is that the growth rates are low and the grown crystals are small with variable single crystal yield [6]. While seeded growth technique can be adopted to improve the yield of single crystal the transport process needs to be studied carefully to increase the growth rates. The mechanism of the vapor transport process in II-VI semiconductors is different from those of the IV-VI and II-VII$_2$ compounds. Under the ideal condition that the partial pressure of the residual (foreign) gas is zero, this difference is mainly caused by the thermodynamic fact that the predominant vapor

W13
1N-76-TM

PROCEEDINGS REPRINT

Reprinted from

Materials Research in Low Gravity

28–29 July 1997
San Diego, California

SPIE
P
PROCEEDINGS SERIES

Volume 3123

species in equilibrium with the II-VI compounds in the temperature range of interest are atomic species of Group II elements, such as Zn and Cd, and diatomic molecules of Group VI elements[10-16], i.e., S_2, Se_2 and Te_2, whereas those for IV-VI compounds under metal (Group IV) saturated conditions are the congruent subliming molecular species such as PbTe [17-19], SnTe [19-21] and GeTe [19] and the predominant vapor species for II-VII$_2$ compounds are HgI_2 and $HgCl_2$ [22]. In the latter case, i.e. when the predominant species is the congruent subliming molecule, the transport process can be described as the diffusion of the congruent subliming species from the source material through a stagnant residual gas to the deposited crystal [23]. Therefore, the transport rate is controlled mainly by the temperatures of the source and the deposition. In the former case, the partial pressures of the species II and VI$_2$ in equilibrium with the II-VI semiconducting compounds, at a fixed temperature, can vary by orders of magnitude as the composition of the compound varying over the narrow homogeneity range from Group II saturation to Group VI saturation[12,13,16]. As a result, the transport rate of the vapor species can also vary from a maximum transport rate corresponding to the condition of congruent sublimation, i.e., the compositions of the solid phase and the equilibrium vapor phase are the same, to transport rates which are orders of magnitude lower when the solid composition deviates significantly from the congruent sublimation. Generally speaking, in the growth temperature range usually adopted the congruent sublimation condition does exist inside the homogeneity range of these II-VI materials [13,16] but a precise control of the stoichiometry of the starting compound from the weighing of the constituent elements is practically impossible. However, with certain heat treatment methods the partial pressures over the starting compound material can be reasonably reproduced.

In Section II, a theoretical calculation of the transport rates for the II-VI compounds using a one-dimensional diffusion model will be presented and the calculated transport rates are basically determined by four parameters — the temperatures at the source and the deposition, the ratio of the partial pressures over the source and the partial pressure of the residual gas. In Section III, the experimental heat treatment methods which control the partial pressures of the staring materials will be discussed. The effectiveness of the heat treatment methods was studied by partial pressure measurements using optical absorption technique which will be the subject of Section IV. Also in section IV, the measurements on the pressure and the compositions of the residual gas by a total pressure gauge technique will be presented. In Section V, an in-situ dynamic technique for the transport rate measurements will be described and a further extension of this technique which simultaneously measures the partial pressures and the transport rate will also be included. The crystal growth experiments will be presented in Section VI which describes the furnace design, the growth parameters and the advantages of the process. A brief discussion of the characterization process, which emphasizes on the analysis of the crystalline structural defects, will be given in Section VII. The paper will be concluded with Discussion in Section VIII.

II. Theoretical Calculation — One Dimensional Diffusion Analysis

The crystal growth of PVT consists of essentially three processes: the sublimation of the source material into vapor species, the transport of the vapor species from the source region to the deposition region, and the condensation of the vapor species to form crystal. For the II-VI compounds, vapor transport is the rate-limiting process under most of the crystal growth conditions. Since the equilibrium vapor pressures over these II-VI compounds are relatively low (10^{-3}–10^{-2} atm) [10-16] at the usual growth temperatures, the small convective contribution to the mass transport in these PVT system can be neglected. The process can, therefore, be well described by a one-dimensional diffusion limited analysis. The theory of diffusion in ideal multispecies gases was developed about a century ago mainly by Maxwell and Stefan. The original form of a Maxwell equation for diffusion of species A through species B was

$$-dP_A = \alpha_{AB} \frac{\rho_A \rho_B}{M_A M_B} (u_A - u_B) \, dy \, ,$$

where P_A is the partial pressure of A along the distance y, ρ's the partial densities, M's the molecular weights, u's the velocities of the species in the direction of net diffusion, and α_{AB} a proportionality constant. Conventionally, the mass flux, or the rate of diffusion of the species A in moles per unit time per unit area, $J_A = u_A \rho_A / M_A$ is used and for a multispecies system we have Maxwell equations of the form

$$-\frac{dP_i}{dy} = \sum_{j \neq i} r_{ij} (J_i P_j - J_j P_i) \, , \, i = A, B, \ldots \qquad (1)$$

where $r_{ij} = \alpha_{ij}/RT = RT/D_{ij}P$, $r_{ij} = r_{ji}$, and D_{ij} is the binary diffusion coefficients. Eq. (1) is accurate only when the temperature, T, and total pressure, P, are constant throughout the volume in which the diffusion takes place. For the PVT growth process of a wide band gap II-VI compound, the total pressure maintains constant throughout the ampoule because of a extremely short mean-free-path of the mole-

cules. The temperature difference commonly experienced between the source material and the grown crystal, 10 to 20°C, is small compared to the absolute temperatures used for the process. Therefore, Eq. (1) has been used satisfactorily to describe the mass transport of these systems.

When in equilibrium, the metal component forms only monomers while the chalcogens are dominated by dimers in the vapor phase. All the other thermodynamically possible chalcogen monomers or polymers have partial pressures at least 2 orders of magnitude lower than that of the corresponding dimers. Therefore, only metal monomer and chalcogen dimer need to be considered in the analysis. Another interesting thermodynamic property for the II-VI compounds is that the Gibbs free energy of formation for the vapor phase is, within experimental error, independent of the deviation from stoichiometry and a function of temperature only. Table 1 lists the parameters of the equilibrium constant K(T) for the various systems.

In the PVT process, a binary compound $A^{II}B^{VI}$ sublimes dissociatively according to the following reaction:

$$AB(s) \rightarrow A(g) + \frac{1}{2}B_2(g) . \tag{2}$$
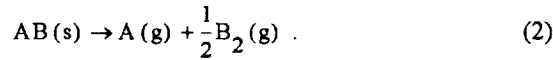
Two Maxwell equations need to be solved. A correlation between two fluxes has to be assumed in order to solve them since only one of the equations is independent due to the constant total-pressure condition. Obviously, $J=J_A=2J_B$ ($B \equiv B_2$ in subscript) is justified because of the fact that all the II–VI compounds have very narrow homogeneity range and no secondary phase was observed in the grown crystals. Using this and $P = P_A + P_B$, the two Maxwell equations can be decoupled and reduced to

$$J = \frac{3}{2}\frac{J}{P}P_A - \frac{1}{r_{AB}P}\frac{dP_A}{dy} , \tag{3}$$

$$J = 3\frac{J}{P}P_B - \frac{2}{r_{AB}P}\frac{dP_B}{dy} \tag{4}$$

respectively. Eqs. (3) and (4) are equivalent to those derived by Faktor and Garrett [24] where the first term on the right-hand side is called the Stefan flow term. The integration of Eqs. (3) and (4) leads to

$$P_A(y) = \frac{2}{3}P + \left[P_A(L) - \frac{2}{3}P\right]\exp\left[\frac{3}{2}Jr_{AB}(L-y)\right] , \tag{5}$$

$$P_B(y) = \frac{1}{3}P + \left[P_B(L) - \frac{1}{3}P\right]\exp\left[\frac{3}{2}Jr_{AB}(L-y)\right]; \tag{6}$$

and

$$J = \frac{2}{3}\frac{D_{AB}P}{RTL}\ln\frac{P_A(0) - \frac{2}{3}P}{P_A(L) - \frac{2}{3}P} = \frac{2}{3}\frac{D_{AB}P}{RTL}\ln\frac{P_B(0) - \frac{1}{3}P}{P_B(L) - \frac{1}{3}P} , \tag{7}$$

in which y=L is where the source is located, 0 is where the crystal is, and J is positive (In Eqs. (1), (3), and (4), the flux is defined as positive in the positive y-direction. When considering a transport from L to 0 the flux becomes negative. However, we still use a positive J here by having adjusted the signs in Eqs. (5)–(7)). Eq. (7) has been used by Su [25] and Sha et al [11] to analyze the CdS and ZnSe system, respectively. Figure 1 shows the results calculated from Eq. (7) for the mass flux in ZnSe system as a function of $\Delta T \equiv T(L) - T(0)$ for different stoichiometries of the source. The binary diffusion coefficients were computed from the Chapman-Enskog formula using the collision integral given by Neufield et al [26]. From Eq. (7), one can find that when $P_A=(2/3)P$, or equivalently $\alpha(L)=P_A(L)/P_B(L)=2$, the flux J is infinite. This condition was also quoted in literature as P_{min} because it corresponds to a minimum in the total pressure. A good discussion on this was given in Ref. [24].

In a real PVT process, however, volatile impurities such as H_2, H_2O, CO, CO_2, N_2, and O_2 may be present resulting from the outgassing of the silica ampoule and/or from source material [27] and form a significant amount of residual gas. Systematic studies have been reported [28-30] on the residual gas formation in sealed silica ampoules. Since these residual species remain in the vapor phase, a third, stagnant component should be included in the diffusion analysis. Faktor and Garrett [24] gave an approximate treatment similar to the one for the two-species problem, which is valid only when the stagnant component is dominant and all three binary diffusion coefficients are equal. The analytical solutions to the Maxwell equations for a three-species problem were first given by Gilliland [31] and can be derived in the following way:

The third equation can be decoupled by setting $J_Z=0$ with Z standing for the residual gas component which represents all the residual species in the vapor phase other than the two transport species (A and B_2) and whose molecular parameters can be calculated as

weighted averages based on the composition of the residual gas. Using $P_Z = P - P_A - P_B$ and $r_{ij}=RT/D_{ij}P$, we have

$$\frac{J_A}{D_{AZ}} + \frac{J_B}{D_{BZ}} = \frac{P}{RT(L-y)} \ln \frac{P_Z(y)}{P_Z(L)} , \qquad (8)$$

$$\frac{J_A + J_B}{D_{AB}} = \frac{P}{RT(L-y)} \ln \frac{(1+J_B/J_A)P_A(y) - a(1+J_A/J_B)P_B(y) - b}{(1+J_B/J_A)P_A(L) - a(1+J_A/J_B)P_B(L) - b} , \qquad (9)$$

where

$$a = \frac{r_{AB} - r_{AZ}}{r_{AB} - r_{BZ}}, \qquad b = \frac{r_{AZ} - r_{BZ}}{r_{AB} - r_{BZ}} P \qquad (10)$$

Again, $J=J_A=2J_B$ should be used in the calculation. Eqs. (8) and (9) have been used by Sha et al [11] and Palosz et al [32] to analyze the mass transport in the PVT systems of ZnSe and CdTe, respectively.

For the given values of T(L), T(0), and α(L), P_A(L) and P_B(L) are calculated from the equilibrium condition $P_A(L)P_B^{1/2}(L) = K(T(L))$. Then $P_A(0)$, $P_B(0)$, $P_Z(0)$, and the mass flux J can be solved from Eqs. (8) and (9) with y=0, $P_A(0)P_B^{1/2}(0) = K(T(0))$, and the constant total-pressure condition with an input value of P_Z(L). The second step can be repeated for different P_Z(L) until the average residual pressure, $\overline{P_Z} = \frac{1}{L}\int_0^L P_Z(y)\,dy$, matches the experimentally determined pressure of the residual gas.

Figure 2 shows the results calculated for the mass flux in the ZnSe-residual gas system as a function of P_Z(L) for different stoichiometries of the source. The residual pressure used, 0.008 atm, was a typical value measured by a total pressure gauge technique described later. The curves in Figure 2 indicate that the residual gas starts to measurably reduce the mass flux when its total pressure approaches the excess pressure $|P_A-2P_B|$. Beyond this region, the residual gas becomes the rate-limiting factor and the α(L)-dependence of the flux becomes weak.

III. Heat Treatments of Starting Materials

The calculation of last section clearly indicates that the vapor transport rate for a binary system is at its maximum when the source material sublimes congruently, i.e., the vapor phase has the same composition as the solid phase. Since the vapor partial pressures coexisting with the solid phase depends strongly on the deviation from stoichiometry of the solid, it is practically impossible to synthesize the starting material with the desired values of partial pressures by weighing of the constituent elements. One method to adjust the stoichiometry of the starting material is to bake out the material at the processing temperature under dynamic vacuum condition (method A). Besides purifying the material by preferentially subliming moisture and other volatile impurities, the process changes the stoichiometry of the starting material until the material sublimes congruently. The disadvantages of the method is the loss of the material at a relatively rapid rate thus the duration of the baking process has to be optimized. The other method is, after the application of method A, to distill the material by sublimation from one end of the ampoule to the other under dynamic vacuum (method B). Piper and Polich [33] baked their CdS starting material under vacuum condition and then annealed it under a stream of H_2S gas. Catano and Kun [34] removed excess Zn in their ZnSe starting material by annealing it under a flow of 1% H_2Se and 99% H_2 and then baked the ZnSe under vacuum. Kaldis [35] reduced his ZnSe starting material by baking it in dry H_2 atmosphere. Ohno et al. [36] heat treated the ZnS starting material by baking it 850°C under vacuum for 12 h then in H_2S atmosphere at the same temperature for 4 h. Burr and Woods [37] essentially heat treated their ZnSe starting materials by method B.

The heat treatment of baking under dynamic vacuum for a binary compound, in principle, only results in the congruent sublimation condition, i.e. α=2.0. To prepare a binary material with a other than 2, a two-zone annealing technique can be adopted. In this setup, the starting material at one temperature is in equilibrium with a predetermined vapor pressure of one of the elements provided by a reservoir at another temperature. Because of the stoichiometric invariant, $RT\ln P_A P_{B_2} = \mu_{AB}(T)$, the system variables are fixed once the temperature and one of the partial pressure are known. The technique can be extended to control the stoichiometry during the transport rate or crystal growth experiment using an in-situ heat treatment of the materials by controlling the partial pressure of one of the constituent element in the growth system. Usually, a three-zone furnace setup is employed where the temperatures of the source, the crystal (deposit) and the reservoir for the element are independently controlled. Prior [38] studied the seedless crystal growth of PbSe under controlled pressures of selenium. The group at Tohoku University, Japan, has investigated the effects of controlled over pressures on the transport rate and crystal growth of CdTe [39-42] and ZnSe [43]. Hoschl and Konak [44] grew crystals of CdTe and CdSe under controlled vapor pressures of one of the components. The group at University of Durham, England, has also studied the crystal growth of

10

ZnSe [37,45], and CdS [46] under a controlled pressure of one of the constituent elements. In principle, the thermodynamic characteristics of these systems is well defined when (1) the amount of the element in the reservoir is large enough such that the chemical potential of the element remains the same as that of the pure element during the experiments and (2) the time is long enough for each step of the process so that the system is in steady state condition throughout the run.

IV. Partial Pressure Measurements

The mass flux in PVT process strongly depends on the partial pressures of the individual transport species as well as the partial pressure of the residual gas. Using the optical absorption technique, Brebrick and co-workers have reported the partial pressure data over the systems of HgTe [47,48], HgSe [49], CdTe [15], ZnTe [12], ZnSe [11,12], PbTe [17,18], SnTe [20,21], PbSnTe [21], HgCdTe [50-52] and HgZnTe [53]. The basic principles for the measurements and the experimental procedure were described in detail in the references above. In brief, the T-shape cell for the optical measurement was made of fused silica. The sample beam of a double beam monochromator passed through the optical windows on the top of the T which was held at a fixed temperature and the sample was located at the bottom of the vertical leg of the T and held at one of a set of temperatures lower than the optical path temperature for measurement. The optical absorbance was measured between 190 and 800 nm and the partial pressures of individual vapor species were calculated using the data of calibration runs for pure elements.

The vapor compositions over the starting materials for several CdTe and ZnSe ampoules were measured by the optical absorption technique. The effectiveness of the heat treatment by baking out under dynamic vacuum (method A) was confirmed by the partial pressure measurements as illustrated in Figure 3. Six batches of CdTe (total weights of 130 to 165 g) were synthesized from pure elements which were weighed to an accuracy of 0.1 mg to have the same number of moles of Cd and Te. The partial pressure of Te_2 at 870°C was determined for samples taken from each batch of as-synthesized material as well as samples that were baked for 8 min under dynamic vacuum at 870°C. The partial pressure ratio, $\alpha = P_{Cd}/P_{Te_2}$, was labeled next to each data point and $\alpha = 2.0$ corresponds to the condition of congruent sublimation. The values of α for the as-synthesized samples were always lower than 2, i.e. Te-rich, and ranged from 8×10^{-3} to 1.92 whereas those for the heat treated samples ranged from 1.84 to 3.09, relatively close to 2. Measurements on three ZnSe optical cells were performed over a range of temperature. Because of the preferential loss of Zn to the vapor phase from the Zn-rich source and the small amounts of ZnSe materials loaded the measured α values for two of the ZnSe cells change from about 5 at 980°C to 2.7 at 1130°C.

The pressure and composition of residual gas were measured after the transport experiment. The technique and the apparatus for the measurement was described in Ref [30]. Briefly, the processed ampoule was placed in a vacuum chamber connected to a pressure gauge and a high vacuum system. After outgassing the chamber and the ampoule at room temperature under high vacuum, the valve between the chamber and the vacuum system was closed. Then, the ampoule was slid and broken and the pressure change in the chamber was recorded. The original pressure in the sealed ampoule was calculated based on the chamber-to-ampoule volume ratio. Determination of the gas composition was made by selectively freeze-out of the gas components in the cold finger cooled to a predetermined temperature with appropriate cold bath mixtures. For temperatures below 77 K, the tip of the cold finger was placed in a stream of liquid helium droplets and the changes in the pressure as a function of temperature were recorded. Based on the literature [27], it has been assumed that the residual gas may consist of H_2, H_2O, CO, CO_2, N_2, and O_2 molecules. The amount of CO, N_2, and O_2 could not be determined separately by this technique. From the mass spectroscopic studies [54,55], the presence of O_2 in residual gas can be ignored. Also, the presence of H_2 in most of our ampoules precludes the simultaneous presence of O_2 at elevated temperatures. For these reasons it was assumed that the amount of O_2 in the residual gas under our experimental condition is negligible. Table 2 lists the pressures and the compositions of several ampoules after the transport process. The starting materials for the first 5 ampoules listed were ground and heat treated by either method A or B. The majority species is CO_2 which accounts for 28–43% of the total except for the ZSTO-3 ampoule. CO and N_2, being indistinguishable in the measuring technique, together, contributed 97% in the ZSTO-3 ampoule and 35–64% in the others. In Ref [30], empty ampoules made of silica glass from various vendors were cleaned and sealed under vacuum and the pressure and composition of the residual gas were measured after the ampoules have been heat treated by different procedures. The results show that the measured residual gas pressure was in the range of 0.085 to 0.32×10^{-3} atm at room temperature for three different silica brands, GE-214, ST-10 and HLQ-210, after the ampoules were outgassed at 1080°C for 16 h and annealed at 1080°C for 168 h. The silica tubing used for the ZnSe transport measurements were GE-214 and the ampoules were outgassed at 1060°C for 16 h before a process of the transport rate measurements typically at 1100°C for 7 days. The comparison of the residual gas pressures between the ZnSe processed ampoules and the GE-214 ampoules heat treated under similar conditions but without the presence of ZnSe, as listed in Table 2, indicates that the total residual pressures in the ZnSe ampoules are about one order of magnitude or more higher. The facts that

the gas composition of the ZnSe ampoules is dominated by carbon oxides (CO and CO_2) whereas that of the empty ampoules consists mainly of hydrogen and water implies that the ZnSe starting material was the potential source of carbon and oxygen in these processed ZnSe ampoules. This is evidenced from the results of two samples, ZST-13 and -15. The sample in ZST-13 was chunky and was heat treated by method A whereas the sample in ZST-15 was ground and heat treated first with H_2 reduction and then by method A. The residual gas pressures listed in Table 2 indicate (1) oxygen was picked up by the ground sample and (2) the extra step of H_2 reduction can reduced the total residual pressure by a factor of 2 to 7.

V. Transport Rate Measurements

Measurements on vapor transport rate have been reported using various technique which can be classified into two categories: (1) visual observation of the linear growth velocity of the deposition in a sealed ampoule inside a transparent furnace for systems such as HgI_2 [56,57], CdTe and PbTe [58] and (2) measurements of the total change in the mass of the source (or the deposition) in a closed ampoule after the transport process has been conducted for a period of time for systems such as the chemical vapor transport of GeSe-GeI_2 [59], the PVT of CdTe [32] and those referred in Section III on the investigation of the effects of controlled over pressures on the transport rate of CdTe [39-42], ZnSe [43], $CdSe_{1-x}S_x$ [60] and $ZnSe_{1-x}S_x$ [61]. The growth temperatures for the materials discussed here are too high to be processed in a transparent furnace which utilizes a gold-plated tubular silica liner to back-reflect the infrared radiation and usually provides a maximum temperature of 900 to 950°C. The disadvantages of the second technique above are: (1) it only yields the average transport rates and (2) the limitation of determining only one data point, i.e. mass flux for a fixed set of T(source) and T(deposit), from each ampoule.

Recently, a continuous measurement of the total mass change in a closed ampoule by an in-situ dynamic technique was developed in our laboratory [11]. A three-zone tubular resistance furnace was employed to perform the transport experiments. A schematic drawing of the setup with a typical temperature profile along the center line of an empty furnace bore are given in Figure 4. Two legs attached to the left end of the ampoule served as a fulcrum. The right end of the ampoule was connected, via a ceramic block, to a ceramic lever which extended out of the furnace and rested on a wire suspended from a Mettler AE 100 electronic balance. The temperatures, T_s at the source and T_d at the deposition, were measured by two thermocouples placed at the ends of the ampoule and together with the balance readings, were recorded by a computer at 15 or 30 min intervals. The balance readings were then converted to the mass transported using the dimensions of the ampoule/lever assembly. These data were plotted versus time and the mass flux was obtained from the slope of the curve. For most of the runs a few different temperature settings were used to determine the dependence of the mass flux on the source temperature. After all the material has transported the accuracy of the measuring system can be confirmed by comparing the total transport mass measured with the total mass loaded and another run using the same ampoule can proceed by simply reversing the temperature gradient.

A series of transport experiments of ZnSe was performed using the in-situ dynamic technique. The results of the mass flux versus the reciprocal of the source temperature from different ampoules are plotted in Figure 5. Each mass flux value was derived from a well defined straight line generally consisting of more than 40 data points on a plot of mass transported vs. time and was normalized to a transport length of 10 cm. With a few exceptions, the ΔT values used ranged from 13 to 20°C. The source materials from Cleveland Crystals, Inc. used for ampoules ZST-2, 4, and 5, shown as solid symbols, display in general lower fluxes with stronger temperature dependence than those of the source materials from Eagle-Picher, Inc., which were used in the other ampoules and shown as open symbols. The methods of heat treatment, method A and B, as described in Section III did not show apparent effect on the measured mass transport rate.

Four parameters are needed, as discussed in Section II, to perform the theoretical calculation for a comparison with the experimentally measured transport rates. The source temperature, T(L), and the average of the pressures and compositions of the residual gas measured from the four experiment ampoules, ZST-6, 7, 9, and 10, listed in Table 2, as given in the caption of Figure 5 were used as input values for two parameters. Two theoretical curves were calculated. The first one is the upper limit for the mass flux and it is calculated with ΔT=18°C and α(L)=2.7 — the lowest value obtained from the partial pressure measurements over two starting materials of ZnSe, as reported in Section IV. And a value of 38 was also measured at 1050°C over the source material of ZST-4. Thus, the lower limit of the mass flux was calculated using ΔT=14°C and α(L)=40. Most of the experimental data fall between these two curves and some agree well with the upper curve which represents the highest mass flux achievable under the experimental conditions. The stronger temperature dependence of some of the measured mass flux than that of the theoretical curves could be caused by a progressive change of the source material toward the congruent sublimation condition as the source temperature increases.

The general agreement observed between the experimental and theoretical results of the mass flux is satisfactory. However, the

actual value of α over the source, or the deposit, during the vapor transport process was not known for these measurements. In principle, this α-value can vary during the transport process because the stoichiometry of the deposit is usually different from that of the source and, therefore, the stoichiometry of the source and that of the deposit, change continuously during the transport process. To have a better understanding of the transport process, a simultaneous in-situ measurement of the transport rates and the partial pressures was designed and performed. The starting material of ZnSe, provided by Eagle-Picher, Inc., was heat treated by distillation under vacuum (method B). After the heat treatment 3 g of ZnSe was loaded into an optical cell, ZSTO-3 and sealed under vacuum. The transport length was 10.3 cm. During the run, the material transported from the reservoir, at 1160°C, to the window end, at 1130°C, with a maximum of 1165°C in between and the partial pressures over the deposited material were measured. The optical absorbance and the balance readings were simultaneously recorded at a 30 min interval. The pressure and compositions of the residual gas were measured after the experiments using the technique described in Section IV. The measured partial pressure of Zn and the mass transported were plotted versus time in Figure 6. The measured optical absorption of Se_2 peaks was too low, due to the combination of the low Se_2 pressure and the short optical path length used, to give accurate measurement of Se_2 pressure. Therefore, the equation for the Gibbs energy of formation listed in Table 1, together with the measured Zn partial pressures were used to calculate the partial pressures of Se_2 which were also plotted in Figure 6. The measured pressures of Zn scattered but remained almost constant throughout the run at about 0.012 atm which corresponds to a value of P_{Zn}/P_{Se_2}, $\alpha=17$. The theoretical flux was calculated using the measured parameters, i.e., thermal field, partial pressures over the deposition and the residual gas pressure and agrees very well with the experimental data as plotted in Figure 6. The measurements of a constant partial pressure of Zn over the duration of the experiment was unexpected. It was speculated that the difference in the stoichiometry for ZnSe under the conditions of α(source)=6.4 (calculated) at 1160°C and α(deposit)=17 at 1130°C are essentially negligible such that the stoichiometry of the ZnSe source remained the same through out the transport experiment.

VI. Crystal Growth

Due to the high melting temperatures, the bulk growth of the wide band gap II-VI semiconducting compounds was mainly performed by vapor growth rather than melt growth. To increase the transport rate and consequently reduce the growth temperature the introduction of a transport agent, such as I_2, was widely employed for CdS [62], ZnSe [34,35,63-68], ZnTe [67], ZnS [36,67,68] and ZnSeS [34,68]. The disadvantage of this chemical vapor transport (CVT) technique is the high level of the unintentional doping of the transport agent [34,64,68]. On the other hand, different variations of the PVT technique have been applied. These variations include the growth in semi-open system [33,69,70] originally developed by Piper and Polich, the stationary seeded growth in a closed system for CdS [71], CdS and CdSe [72], and ZnSe [73], the translational unseed growth in a closed system for CdS [74,75], ZnTe [76,77], ZnSe [78-80] as well as seeded growth for CdTe [81] and the growth of CdS [46,82,83], ZnSe [37,45,84], ZnSeS [61] and CdSeS [60] under the controlled partial pressure of one (or two) of the constituent elements in a closed ampoule. The thermally induced strain and defects caused by the crucible wall was eliminated in the seeded contactless growth of CdS and CdSe reported in Ref. [71,72] and in a novel self-seeded contactless growth of CdTe [85]. The growth of doped-ZnTe by introducing small amount of In into the growth system was also reported [86].

In our laboratory, the growth activities were concentrated on the translational growth in a closed system, seeded as well as unseeded, for its experimental simplicity and minimal needs for process control in the microgravity environment of space. After the transport rate was optimized the crystal growth proceeded with the judicious choices of the growth parameters. Usually, the heat treatment technique which resulted in the highest transport rate was adopted. As shown in Figure 4, the mass fluxes are almost saturated to the maxima when $\Delta T=20$°C for those values of a close to 2.0. Therefore, the furnace, or the ampoule, translation rate was selected to be close to but slower than the measured transport rate for a ΔT of 15 to 20°C. It was also believed that a slow but practical transport rate improves the morphological and crystalline quality of the grown crystals [73] and, therefore, in some cases inert gas was intentionally introduced into the system [55]. Both unseeded and seeded growth experiments were performed. The compositions of the vapor species in the growth ampoules can be determined by the optical absorption technique. For unseeded growth condition, this can be accomplished by using the ampoule design as shown in Figure 7. The material will be transported to the optical window end after the partial pressure measurements and then the crystal growth will start at the tapered end. Figure 7 also shows the ampoule design for seeded growth experiments. In the determination of the vapor pressure the procedure is the same as the unseeded condition. After the pressure measurements, the ampoule will be opened and seed, quartz wool, and a quartz rod will be loaded as shown. The ampoule is then sealed under vacuum.

Figure 7 also illustrates a typical temperature profile and the initial ampoule positions during a growth run [75,76]. The profile can be easily provided by a three-zone furnace with an adiabatic zone inserted between the central and the end zones. The temperature pro-

file translates to the right during the growth. For the unseeded situation, the crystal starts to nucleate when the ampoule tip is at the supercooling position with a temperature lower than the thermal supersaturation as shown in Figure 7. In the case of the seeded growth, the initial ampoule position needs to be carefully adjusted such that the middle section of the seed is positioned at the supercooling position. Under such condition, part of the seed sublimes first and then the grown crystal nucleates and grows on top of the seed.

A three-zone tubular resistance furnace was used to produce a sharp gradient which resulted in a well-defined position for the supersaturated vapor phase and consequently, a well-defined solid-vapor interface. Using this method, large crystals of CdS [75], ZnTe [76], CdTe, PbSe, and ZnSe [81] have been grown consistently. In most of the runs, the interface of the growth crystals vary from concave (towards the crystal) for CdTe, to almost flat for ZnTe and PbSe, to slightly convex for CdS and convex for ZnSe crystals. To achieve the monocrystalline growth the precise control of the growth interface shape is critical. It is believed that a slight convex interface not only promotes favorable crystalline grain selection, eliminates the nucleation of undesirable secondary grains, also causes existing extended defects to grow towards the container wall and be eliminated, and minimizes thermally induced defects. After analyzing the thermal environment near the interface, the low thermal conductivity of the CdTe solid was considered to be the main reason for the shape of the interface. To modify the thermal environment an adiabatic zone (2.5 to 5 cm thick) made of ceramic was inserted between the central heater and the cold zone. This resulted in an improvement of the CdTe growth interface to a flat surface.

In the simple case of vapor transport experiment the onset location and the length of the deposition region depend on the temperature and partial pressure distributions along the length of the ampoule. The driving force for the growth (deposition) is the free energy change of the reaction corresponding to the vapor-solid growth process. As demonstrated in the HgZnTe-HgI$_2$ chemical vapor transport system [87], the location of the deposition zone can be predicted when the temperature and partial pressure profiles along the ampoule are well defined. In the growth system discussed here the degree of supercooling depends not only on the temperature and partial pressure distributions but also on the vapor transport rate of the source material and the furnace translation rate. In the simple case that the furnace remains stationary the partial pressure profiles can be calculated only when the stoichiometry, or the value of α, of the source is known. With a fixed furnace (or ampoule) translation rate one has to consider whether the degree of supercooling ΔT can provide a mass flux fast enough to keep up with the translation rate.

The advantages of the temperature distribution used here for crystal growth are the following.

1. The peak in the thermal profile provides confinement of the region of supersaturation to a narrow region because of the high temperature gradient at the growth interface.

2. The peak in the profile also eliminates possible secondary nucleation sites by desorbing inadvertently deposited material from the ampoule wall just ahead of the crystal/vapor growth interface.

3. Use of furnace (or ampoule) translation assures that the position of super- saturation can and will be maintained at the growth interface throughout the growth of the entire crystal.

4. The use of the insulation (or adiabatic) zone allows for precise control of the growth interface shape which promotes favorable crystalline grain selection, eliminates the nucleation of undesirable secondary grains, causes existing extended defects to grow toward the container wall and be eliminated, and minimizes thermally induced defects.

5. The generation of crystal defects usually results from the low yield strength at the high growth temperatures required to achieve monocrystal growth. The yield strengths of materials in general rapidly increase with decreasing temperature. With the method and apparatus described here, growth can be accomplished at temperatures lower than commonly used. This allows the production of crystals with a higher degree of perfection because of the increased crystal yield strength.

VII. Characterization

Extensive characterization technique on the grown crystals has been reported and will not be discussed in detail here. In general, these technique were applied to characterize the crystalline structural properties as well as the electrical and optical properties of the grown crystals. In our laboratory, the studies on the structural defects, including impurities, voids, precipitates, dislocations, slip bands, small angle grain boundaries, twins and compositional variation in ternary compounds were accomplished by various technique such as Spectroscopy (atomic absorption and spark source mass spectroscopy), X-ray diffraction (Laue reflection and rocking curve), synchrotron radiation images of white X-ray beam (reflection and transmission), Microscopy (optical, electron, and atomic force), sample polishing and etching and optical transmission. The electrical and optical characterization was performed by optical transmission, photoluminescence, and Hall measurements.

Figure 8 shows the flow chart of the material preparation and characterization technique practiced in this investigation. The characterization results on the wide band gap II-VI semiconductors are reported briefly below.

1. Microscopy. Optical and electron microscopy were employed to study growth surface morphology and structural defects (after appropriate chemical etching) such as voids, precipitates, dislocations, small angle grain boundaries and twins. The ZnSe crystals cleave easily along (110) planes which are also the planes that growth facet developed. The morphology of freshly cleaved surfaces of a ZnSe crystal was examined by AFM [88] and particles with the size of about 20 nm were observed and identified by differential scanning calorimetry [88] to be Se-rich eutectic. Some segregation effect of the precipitates along low angle grain boundaries was evident. However, in the ZnSe crystals grown from the source materials provided by other vendor and under different thermal conditions the Se-rich precipitates were not observed.

2. X-ray Laue diffraction. The growth orientations of unseeded single crystals were routinely determined by X-ray Laue technique. Cutter et al. [85] reported that the growth surfaces of ZnSe crystals have tendency to be close to the (111)B (Se face) plane. Our preliminary results indicate a random preference for the growth orientation.

3. Optical absorption. The room temperature measurement of optical absorption spectra is a convenient yet accurate method for the compositional mapping of a ternary semiconducting wafer [89]. The low temperature (4.2 K) infrared absorption measurements was used to detect the impurity absorption in the crystal [76,90]. Absorption peaks of Cu impurity were observed in ZnTe crystals grown by traveling heater method (THM) but were not observed in the ZnTe grown by PVT technique and the spectra of the Cu absorption peaks were interpreted on the basis of crystal field theory with a dynamic Jahn-Teller interaction acting on the excited states [90].

4. Synchrotron white beam X-ray topography (SWBXT). An overall mapping of the structural defects in a crystal wafer can be easily provided by the SWBXT technique. Recently, (111) wafers sliced from a ZnTe crystal grown by PVT were characterized by this technique [76,91,92]. The topography images in the transmission mode revealed the presence of dislocation slip bands, subgrain structures and long, thin 180° rotational twin lamella. The initiation of slip at regions of stress concentration, such as the lateral twin boundaries, the junctions of subgrain boundaries and twin boundaries was also revealed. The chronological growth history of the crystal and the possible mechanisms for the production of a long, thin twin lamella were deduced from the SWBXT images of a series of wafers sliced from one ZnTe crystal [92]. The SWBXT images of the ZnSe wafers have different features from that observed on the ZnTe wafers. Although long, thin twins were still present, instead of the cellular subgrain structure the SWBXT images of the ZnSe wafers show network of slip bands along three (111) slip planes.

5. Photoluminescence (PL). The presence of Cu impurity, as a substitutional acceptor, was also confirmed by PL measurements at 10.6 K [93] in the ZnTe crystals grown by both PVT and THM. The THM ZnTe crystals were found to contain more Cu impurity than the PVT ZnTe crystals as one would expect from the purification function of the PVT process. The formation of Cu_{Zn}-V_{Te} complexes and the effects of annealing, oxygen contamination and intentional Cu doping were also studied [93]. The effects of post-growth annealing of CdS in Cd and S over pressures were also investigated by PL on two types of as-grown crystals, one "dark" and the other "clear" and a model for the mechanism of the native defect formation was discussed [94].

VIII. Discussion

Both theoretical and experimental results demonstrate the importance of the control in the starting material stoichiometry to the transport rate and consequently the growth process. The heat treatment of the starting materials discussed here provides starting materials with a reproducible stoichiometry. However, the transport rate can also be limited by the residual gas pressure. The analysis of the composition of the residual gas implies that the potential source of the carbon and oxygen observed in the residual gas was the starting materials. The heat treatment process of flowing hydrogen over the source materials at elevated temperature can reduce the oxygen content, lower the residual gas pressure and, consequently, increase the growth rate.

In-situ measurements, such as the simultaneous measurements of partial pressures and the transport rates described, has furthered our understandings of the vapor species transport mechanism. On the other hand, the issues on the growth process and the kinetics at the growth interface such as how do the group VI dimers decompose into atoms, how is the molecular structure formed — is it formed in the vapor phase first or on the crystal surface directly, what are the effects of the surface diffusion and re-vaporization of material on the forming of crystals and, consequently, what are the effects of surface morphology in the atomic scale on the kinetics and the crystallization process of the crystals, etc., have not been understood at this time. The deposition rates in the epitaxial growth of ZnSe on GaAs vary from 0.2 mm/h on a (111)A substrate to 0.5 mm/h on a (111)B and 0.97 mm/h on a (112) substrate [64] implies that not only the surface morphology but also the surface chemistry is playing a role in the deposition kinetics. The origin of the commonly

observed 180° rotating twins in ZnTe and ZnSe grown crystals was not known. In the vapor phase epitaxy (basically, seeded PVT) growth of CdTe on CdTe substrates Yoshioka et al. [95] found that twinned crystals of CdTe only grow on (111) substrates and do not grow on (211) surfaces and they speculated as follows. A (211) plane in a macroscopic sense consists of many (111) planes with steps between them and these steps define the atomic arrangement of the adsorbed molecules uniquely so that grown layers do not give twin crystals. On the other hand, the growth on the (111) face is a two-dimensional nucleation process and the nuclei can have two opposite orientations because of the freedom in rotation. More research and investigation are needed to confirm the speculation. In-situ technique used in the MBE and MOCVD thin film technology to monitor the surface of growing crystals, when modified to fit into the high temperature and high pressure environment of the PVT process, will provide important information in the kinetics and process of the growth and formation of crystal and the mechanism of defect formation.

ACKOWLEDGMENTS

REFERENCES:

[1] for example: Morkoc, H., Strite, S., Gao, G. B., Lin, M.E., Sverdlov, B. & Burns, M. 1994, J. Appl. Phys. 76, 1363; Krasnov, A. N., Purtov, Yu. N., Vaksman, Yu. F. & Serdyuk, V. V. 1992, J. Crystal Growth 125, 373; Kukimoto, H. 1991, Semicond. Sci. Technol. 6, A14.

[2] for example: Yang, X. H., Hays, J. M., Shan, W., Song, J. J. & Cantwell, E. 1993, Appl. Phys. Lett. 62, 1072; Jeon, H., Ding, J., Nurmikko, A. V., Xie, W., Grillo, D. C., Kobayashi, M., Gunshor, R. L., Hua, G. C. & Otsuka, N. 1992, Appl. Phys. Lett. 60, 2045; Nakanishi, K., Suemune, I., Fujii, Y., Kuroda, Y. & Yamanishi, M. 1991, Appl. Phys. Lett. 59, 1401; Neumark, G. F., Park, R. M. & Depuydt J. M. 1994, Physics Today, June, 26; Daneu, V., DeGloria, D. P., Sanchez, A., Tong, F. & Osgood, Jr. R. M. 1986, Appl. Phys. Lett. 49, 546.

[3] Howie, J. A. B., Rowles, G. K. & Hawkins, P. 1991, Meas. Sci. Technol. 2, 1070.

[4] for example: Yang, X. H., Hays, J., Shan, W., Song, J. J., Cantwell, E. & Aldridge, J. 1992, Appl. Phys. Lett. 60, 926; Jeon, H., Ding, J., Patterson, W., Nurmikko, A. V., Xie, W., Grillo, D. C., Kobayashi, M. & Gunshor, R. L. 1991, Appl. Phys. Lett. 59, 3619.

[5] Ichino, K., Wu, Y.-H., Kawakami, Y., Fujita, S. & Fujita, S. 1992, J. Crystal Growth 117, 527.

[6] Triboulet, R. 1991, Semicon. Sci. Technol. 6, A18.

[7] Lauck, R., Muller-Vogt, G. & Wendl, W. 1986, J. Crystal Growth 74, 520.

[8] for example: Chernov, A. A., 1974, J. Crystal Growth 24/25, 11; Rosenberger, F., Delong, M. C., Greenwell, D. W., Olson, J. M. & Westphal, G. H. 1975, J. Crystal Growth 29, 49; Xiao, R.-F., Alexander, J. I. & Rosenberger, F. 1990, J. Crystal Growth 100, 313.

[9] Chen, J.-S., Ming, N.-B., Rosenberger, F. 1986, J. Chem. Phys. 84, 2365.

[10] Sharma, R. C. & Chang, Y. A. 1988, J. Crystal Growth 88, 193.

[11] Sha, Y.-G., Su, C.-H., Palosz, W., Volz, M. P., Gillies, D. C., Szofran, F. R., Lehoczky, S. L., Liu, H.-C. & Brebrick, R. F. 1995, J. Crystal Growth 146 42; Su, C.-H., Sha, Y.-G., Mazuruk, K., Lehoczky, S. L., Liu, H.-C., Fang, R. & Brebrick, R. F. 1996, J. Crystal Growth 166, 736.

[12] Brebrick, R. F. & Liu, H. 1996, High Temp. Mater. Sci. 35 215.

[13] Brebrick, R. F. 1969, J. Electrochem. Soc. 116, 1274.

[14] Goldfinger, P. & Jeunehomme, M. 1963, Trans. Faraday Soc. 59, 2851.

[15] Floegel, P. Z. 1969, Anorg. Allg. Chem. 370, 16.

[16] Brebrick, R. F. 1971, J. Electrochem. Soc. 118, 2014.

[17] Huang, Y. & Brebrick, R. F. 1988, J. Electrochem. Soc. 135, 486.

[18] Brebrick, R. F. & Strauss, A. J. 1964, J. Chem. Phys. 40, 3230.

[19] Northrop, D. A. 1971, J. Phys. Chem. 75, 118.

[20] Brebrick, R. F. & Strauss, A. J. 1964, J. Chem. Phys. 41, 197.

[21] Huang, Y. & Brebrick, R. F. 1988, J. Electrochem. Soc. 135, 1547.

[22] JANAF Thermochemical Tables, 1971, NSRDS-NBS, Natl. Bur. Std. (US), Washington, DC, 2nd ed.; Piechotka, M. & Kaldis, E.

1986, J. Less Common Metals 115, 315.

[23] Cadoret, R., Brisson, P. & Magnan, A. 1989, Nucl. Inst. Meth. A283, 339.

[24] Faktor, M. M. & Garrett, I. 1974, Growth of Crystals from the Vapour, Chapman and Hall, London.

[25] Su, C.-H. 1987, J. Crystal Growth 80, 333.

[26] Reid, R. C., Prausnitz, J. M. & Sherwood, T. K. 1977, The Properties of Gases and Liquids, McGraw-Hill, New York, 3rd ed.

[27] for example: Russell, G. J. & Woods, J. 1979, J. Crystal Growth 46, 323; Schmidt, G. & Gruehn, R. 1982, J. Crystal Growth 57, 585; Morimoto, Y., Igarashi, T., Sugahara, H. & Nasu, S. 1992, J. Non-Cryst. Solids 139, 35.

[28] Harman, T. C. & McVittie, J. P. 1974, J. Electron. Mater. 3, 843.

[29] Palosz, W. & Wiedemeier, H. 1993, J. Crystal Growth 131, 193.

[30] Palosz, W., Szofran, F. R. & Lehoczky, S. L. 1994, J. Crystal Growth 142, 215.

[31] Sherwood, T. K. 1937, Absorption and Extraction, McGraw-Hill, New York.

[32] Palosz, W. & Wiedemeier, H. 1993, J. Crystal Growth 129, 653.

[33] Piper, W. & Polich, S. J. 1961, J. Appl. Phys. 32, 1278.

[34] Catano, A. & Kun, Z. K. 1976, J. Crystal Growth 33, 324.

[35] Kaldis, E. 1965, J. Phys. Chem. Solids 26, 1701.

[36] Ohno, T., Kurisu, K. & Taguchi, T. 1990, J. Crystal Growth 99, 737.

[37] Burr, K. F. & Woods, J. 1971, J. Crystal Growth 9, 183.

[38] Prior, A. C. 1961, J. Electrochem. Soc. 108, 82.

[39] Igaki, K., Ohashi, N. & Mochizuki, K. 1976, Jap. J. Appl. Phys. 15, 1429.

[40] Igaki, K. & Mochizuki, K. 1974, J. Crystal Growth 24/25, 162.

[41] Mochizuki, K. 1981, J. Crystal Growth 51, 453.

[42] Mochizuki, K. 1981, J. Crystal Growth 53, 355.

[43] Kiyosawa, T., Igaki, K. & Ohashi, N. 1972, Trans. Jap. Inst. Metals 13, 248.

[44] Hoschl, P. & Konak, C. 1965, Phys. Stat. Sol. 9, 167.

[45] Cutter, J. R. & Woods, J. 1979, J. Crystal Growth 47, 405.

[46] Clark, L. & Woods, J. 1968, J. Crystal Growth 3/4, 126.

[47] Brebrick, R. F. & Strauss, A. J. 1965, J. Phys. Chem. Solids 26, 989.

[48] Su, C.-H., Liao, P.-K., Tung, T. & Brebrick, R. F. 1981, High Temp. Sci. 14, 181.

[49] Brebrick, R. F. 1965, J. Chem. Phys. 43, 3846.

[50] Schwartz, J. P., Tung, T. & Brebrick, R. F. 1981, J. Electrochem. Soc. 128, 438.

[51] Tung, T., Golonka, L. & Brebrick, R. F. 1981, J. Electrochem. Soc. 128, 451.

[52] Su, C.-H., Liao, P.-K. & Brebrick, R. F. 1985, J. Electrochem. Soc. 132, 942.

[53] Chen, K.-T., Sha, Y.-G. & Brebrick, R. F. 1990, J. Vac. Sci. Technol. A8, 1086.

[54] Murray, J. J., Pottie, R. F. & Sander, R. L. 1973, J. Mater. Sci. 8, 37.

[55] Morimoto, Y., Igarashi, T., Sugahara, H. & Nasu, S. 1992, J. Non-Cryst. Solids 139, 35.

[56] Zha, M., Piechotka, M. & Kaldis, E. 1991, J. Crystal Growth 115, 43.

[57] Kaldis, E. & Piechotka, M. 1994, Handbook of Crystal Growth, Vol. 2, Chap. 11, Elsevier Science, North-Holland.

[58] Zoutendyk, J. A. & Akutagawa, W. M. 1982, Mater. Processing in the Reduced Gravity Environment of Space, Elsevier Science, Rindone, G. E. Editor, p. 449.

[59] Wiedemeier, H., Chandra, D. & Klaessic, F. C. 1981, J. Crystal Growth 51, 345.

[60] Mochizuki, K. & Igaki, K. 1978, J. Crystal Growth 45, 218.

[61] Mochizuki, K. 1982, J. Crystal Growth 58, 87.

[62] Kaldis, E. 1969, J. Crystal Growth 5, 376.

[63] Parker, S. 1971, J. Crystal growth 9, 177.

[64] Koyama, T., Yodo, T., Oka, H., Yamashita, K. & Yamasaki, T. 1988, J. Crystal Growth 91, 639.

[65] Recker, K. & Schoepe, R. 1971, J. Crystal Growth 9, 189.

[66] Parker, S. G. & Pinnell, J. E. 1969, Trans. Meta. Soc. AIME 245, 451.

[67] Hartmann, H. 1977, J. Crystal Growth 42, 144.

[68] Fujita, S., Mimoto, H., Takebe, H. & Noguchi, T. 1979, J. Crystal Growth 47, 326.

[69] Russell, G. J. & Woods, J. 1979, J. Crystal Growth 47, 647.

[70] Morimoto, J., Ito, T., Yoshioka, T. & Miyakawa, T. 1982, J. Crystal Growth 57, 362.

[71] Markov, E. V. & Davydov, A. A. 1971, Neorg. Mater. 7, 575.

[72] Davydov, A. A. Ermolov, V. N., Neustroev, S. V. & Pavlova, L. P. 1992, Neorg. Mater. 28, 42.

[73] Cantwell, G., Harsch, W. C., Cotal, H. L., Markey, B. G., McKeever, S. W. S. & Thomas, J. E. 1992, J. Appl. Phys. 71, 2931.

[74] Hemmat, N. & Weinstein, M. 1967, J. Electrochem. Soc. 114, 851.

[75] Su, C.-H., Lehoczky, S. L. & Szofran, F. R. 1990, J. Crystal Growth 101, 221.

[76] Su, C.-H., Volz, M. P., Gillies, D. C., Szofran, F. R., Lehoczky, S. L., Dudley, M., Yao, G.-D. & Zhou, W. 1993, J. Crystal Growth 128, 627.

[77] Taguchi, T., Fujita, S. & Inuishi, Y. 1978, J. Crystal growth 45, 204.

[78] Anderson, E., Cheng, H.-Y. & Edgell, M. J. 1989, Mater. Res. Soc. Symp. Proc. 152, 51.

[79] Cheng, H.-Y. & Anderson, E. 1989, J. Crystal Growth 96, 756.

[80] Allegretti, F., Carrara, A. & Pizzini, S. 1993, J. Crystal Growth 128, 646.

[81] Su, C.-H., Sha, Y.-G., Volz, M. P., Gillies, D. C., Szofran, F. R., Lehoczky, S. L., Zhou, W., Dudley, M., Liu, H.-C., Brebrick, R. F. & Wang, J. C. 1994, Proc. AIAA 32nd Aerospace Sciences Meeting, paper 94-0564.

[82] Russell, G. J., Thompson, N. F. & Woods, J. 1985, J. Crystal Growth 71, 621.

[83] Fochs, P. D., George, W. & Augustus, P. D. 1968, J Crystal Growth 3/4, 122.

[84] Hartmann, H. & Siche, D. 1994, J. Crystal Growth 138, 260.

[85] Grasza, K., Zuzga-Grasza, U., Jedrzejczak, A., Galazka, R. R., Majewski, J., Szadkowski, A. & Grodzicka, E. 1992, J. Crystal Growth 123, 519.

[86] Jordan, A. S. & Derick, L. 1969, J. Electrochem. Soc. 116, 1424.

[87] Sha, Y.-G., Su, C.-H. & Szofran, F. R. 1993, J. Crystal Growth 131, 574.

[88] Chen, K.-T., George, M. A., Zhang, Y., Burger, A., Su, C.-H., Sha, Y.-G., Gillies, D. C. & Lehoczky, S. L. 1995, J. Crystal Growth 147 292.

[89] for example: Su, C.-H., Perry, G. L. E., Szofran, F. R. & Lehoczky, S. L. 1988, J. Crystal Growth 91, 20; Su, C.-H., Lehoczky, S. L. & Szofran, F. R. 1991, J. Crystal Growth 109, 392.

[90] Volz, M. P., Su, C.-H., Lehoczky, S. L. & Szofran, F. R. 1992, Phys. Rev. B46, 76.

[91] Zhou, W., Wu, J., Dudley, M., Su, C.-H., Volz, M. P., Gillies, D. C., Szofran, F. R. & Lehoczky, S. L. 1993, Mater. Res. Soc. Symp. Proc., Infrared Detectors-Materials, Processing, and Devices, Applebaum, A. & Dawson, L. R., Editors, p. 299.

[92] Zhou, W., Dudley, M., Wu, J., Su, C.-H., Volz, M. P., Gillies, D. C., Szofran, F. R. & Lehoczky, S. L. 1994, Mater. Sci. & Eng. B27, 143.

[93] Biao, Y., Azoulay, M., George, M. A., Burger, A., Collins, W. E., Silberman, E., Su, C.-H., Volz, M. E., Szofran, F. R. & Gillies, D. C. 1994, J. Crystal Growth 138, 219.

[94] Chen, K.-T., Zhang, Y., Egarievwe, S. U., George, M. A., Burger, A., Su, C.-H., Sha, Y.-G. & Lehoczky, S. L. 1996, J. Crystal Growth 166, 721.

[95] Yoshioka, Y., Yoda, H. & Kasuga, M. 1991, J. Crystal Growth 115, 705.

Table 1. Parameters for equilibrium constants of various $A^{II}B^{VI}$ compounds

$$\log P_A P_{B_2}^{1/2} \, (\mathrm{atm}) = -C/T + D$$

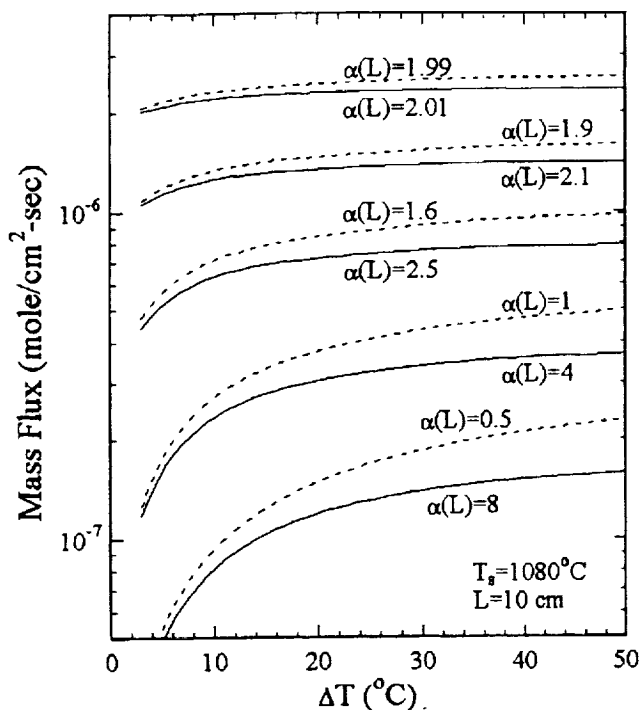| Compounds	C	D	Ref.
ZnS	19942	10.264	[10]
ZnSe	17818	9.1888	[12]
ZnTe	16350	9.680	[13]
CdS	17247	10.466	[14]
CdSe	16632	10.092	[15]
CdTe	15003	9.8224	[16]

Figure 1 Calculated mass flux of ZnSe as a func tion of ΔT for source temperature at 1080°C and different values of α(L). Solid lines are for α(L)>2 and dashed lines for α(L)<2.
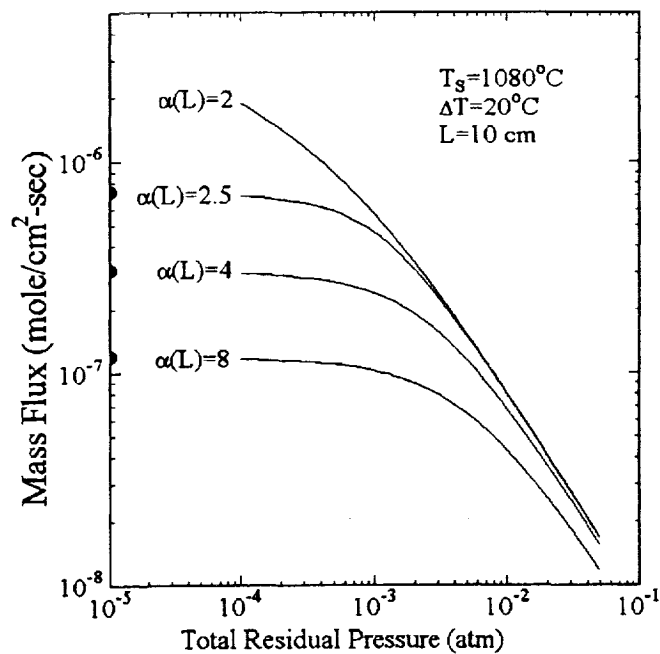
Figure 2 Calculated mass flux of ZnSe as a function of $P_Z(L)$ for source temperature at 1080°C and different values of α(L). The solid dots on the left axis are those under the same conditions but with a zero residual gas pressure.

Table 2 Residual gas in the processed ampoules of ZnSe

Sample	Total Pressure at Room Temperature (atm)	H_2O %	CO_2 %	$CO+N_2$ %	H_2 %
ZST-6[b]	4.132×10^{-3}	<1	30	62	8
ZST-7[b]	1.092×10^{-3}	<1	43	35	21
ZST-9[a]	1.658×10^{-3}	<1	42	48	10
ZST-10[b]	1.947×10^{-3}	<1	28	64	8
ZSTO-3[b]	4.961×10^{-3}	2	0.2	96.5	1.3
Empty[c]	0.23×10^{-3}	40	0	60	0
ZST-13[d]	0.32×10^{-3}	0	53	47	0
ZST-15[e]	0.76×10^{-3}	<1	13	25	61

a. Ground sample, heat treated by baking under dynamic vacuum.
b. Ground sample, heat treated by baking and distillation.
c. Palosz et al. (1994).
d. Chunky sample, heat treated by baking under dynamic vacuum.
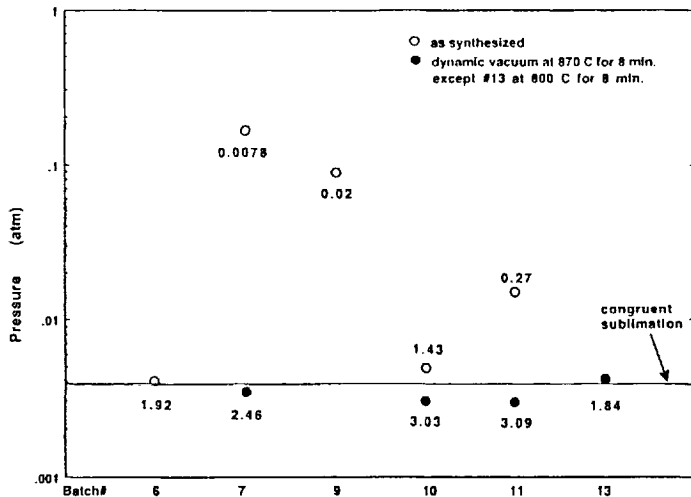e. Ground sample, heat treated with H_2 reduction and dynamic baking under vacuum.

Figure 3 Partial pressure of Te_2 measured at 870°C for different batches of CdTe starting material. Open circles are the results for as-synthesized material and closed circles for the material heat treated by method A. The numbers adjacent to each data point represent the partial pressure ratio, a, and the horizontal line is the P_{Te_2} corresponding to the congruent sublimation, i.e. $\alpha=2.0$, for CdTe at 870°C.
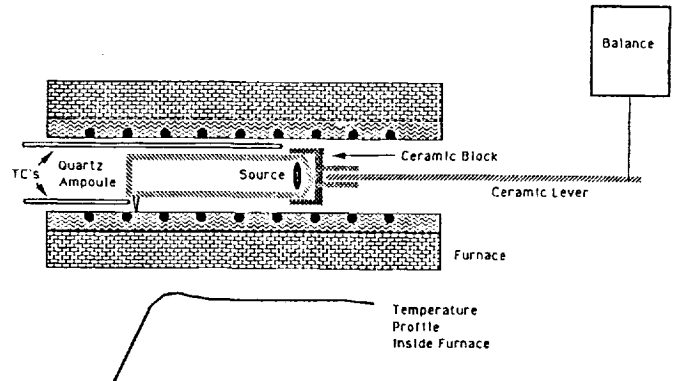
Figure 4 Schematics of the setup for the transport rate measurement by the in-situ dynamic technique.
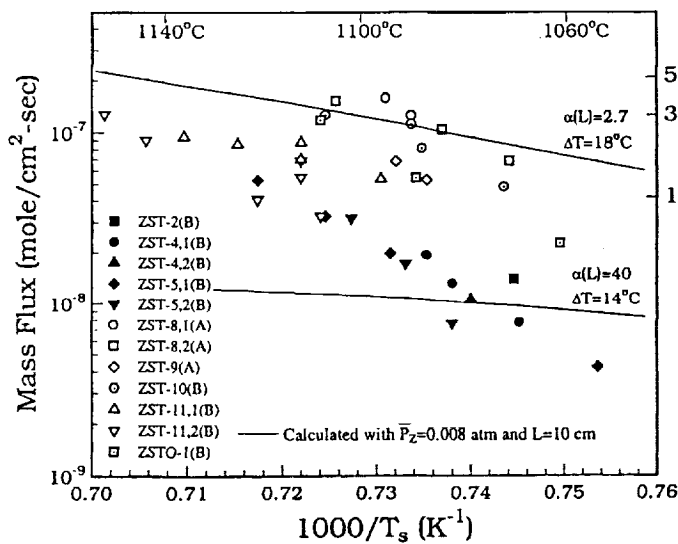
Figure 5 Mass fluxes of ZnSe as a function of reciprocal of source temperature. Solid symbols: source materials from Cleveland Crystals, Inc.; open symbols: source materials from Eagle-Picher, Inc. The letters in the parentheses in legend indicate the method of heat treatment. The solid lines are calculated with conditions described in the text. The composition of the residual gas used in the calculation is 36% CO_2, 26% each for CO and N_2 and 12% H_2.
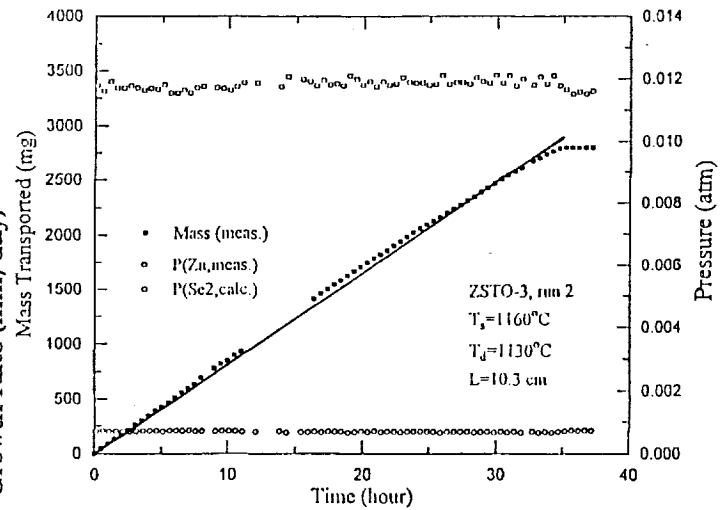

Figure 6 Measured P_{Zn} over the deposit and measured ZnSe mass transported versus time for ZSTO-3. The P_{Se_2} data were calculated from P_{Zn} and the equilibrium constant. The solid line is the calculated mass fluxes for ZSTO-3. The measured pressure and compositions of the residual gas were used in the calculation.
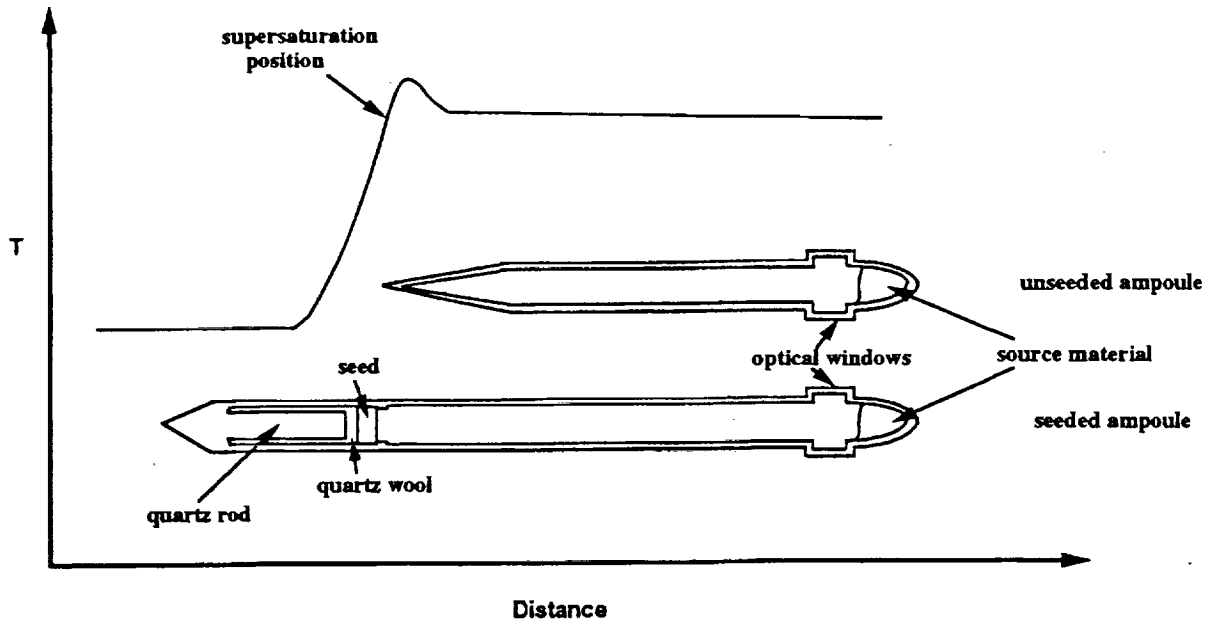
20

Figure 7. Schematics of thermal profile and initial ampoule positions for unseeded and seeded growth
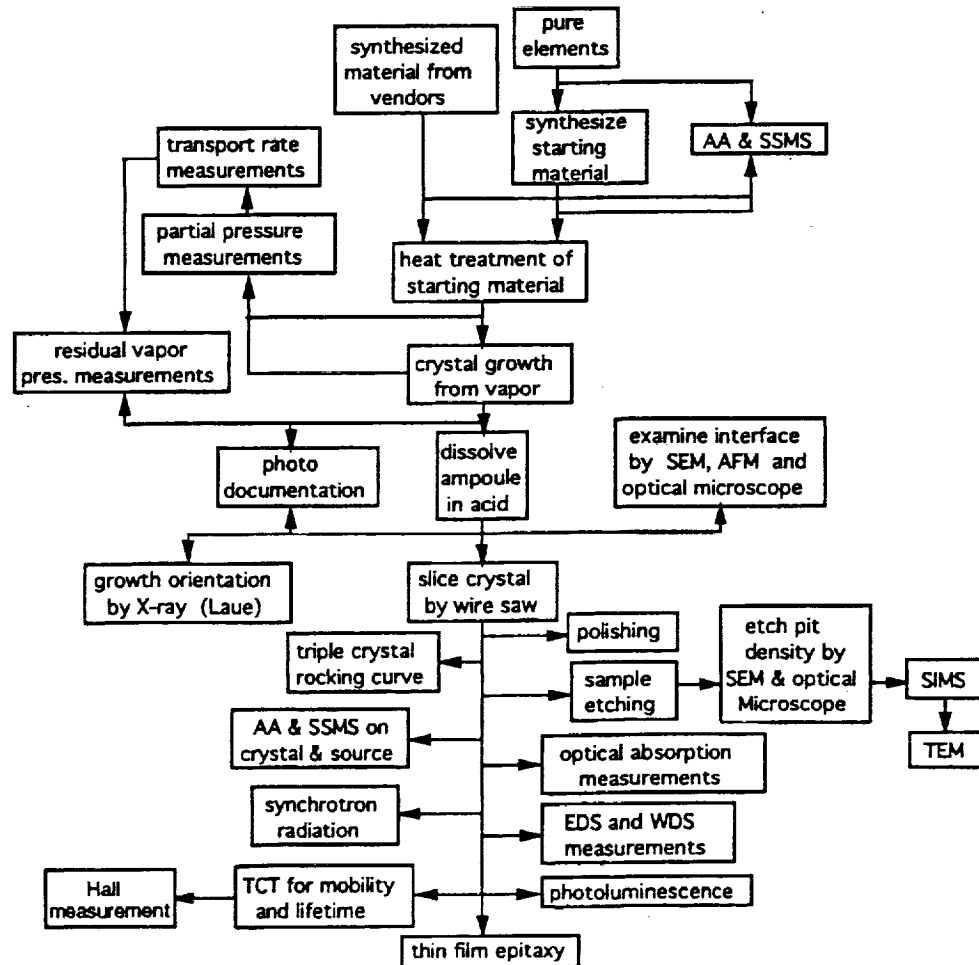

Figure 8. Flow chart of sample preparation and characterization plan